

Simple and rapid methods based microwave and sonochemistry for synthesizing of tellurium nanostructures using novel starting reagents for solar cells

Mokhtar Panahi-Kalamuei · Parisa Rajabpour ·
Masoud Salavati-Niasari · Zabihullah Zarghami ·
Mehdi Mousavi-Kamazani

Received: 8 January 2015 / Accepted: 1 February 2015 / Published online: 10 March 2015
© Springer Science+Business Media New York 2015

Abstract Herein, tellurium (Te) nanostructures were successfully synthesized via microwave and sonochemical routes in which tellurium tetrachloride as a tellurium source and hydrazine, potassium borohydride, and thioglycolic acid (TGA) as reducing reagents were used. TGA can be easily oxidized to the corresponding disulfide [SCH₂CO₂H]₂, which in turn can reduce TeCl₄ to Te. The obtained Te was characterized by XRD, SEM, EDS, and DRS. Additionally, the effects of reducing agent as well as solvent and surfactant on morphology and size of the products were studied. Tellurium thin film was deposited on the FTO–TiO₂ by Dr-blading then employed to solar cell application and measured open circuit voltage (V_{oc}), short circuit current (I_{sc}), and fill factor were determined as well. The studies showed that preparation method play crucial role on particle morphology and sizes. As result, various solar cell efficiencies will be achieved for the obtained nanostructures.

1 Introduction

Tellurium is a p-type semiconductor with direct narrow band gap energy of 0.35 eV at room temperature. It has been employed for piezoelectric devices owing to its non-centrosymmetry [1, 2], high-efficiency conductors

[3], catalytic activities [4], carbon monoxide [5] and ammonia [6] gas sensors. Furthermore, tellurium and its alloys are utilized as significant semiconductor materials for thermoelectric generators and coolers due to their high thermo power [7]. Additionally Te can react with other element to generate many functional materials, such as, ZnTe, CdTe, etc. [8, 9]. So, control of preparation of tellurium nanostructures might introduce new types of application in future nanodevices [10]. During last decades, massive studies have been reported on synthesis routes to obtain Te nanostructures [11–18]; however, very toxic reagents, complex procedures, or very long reaction time are usually needed to synthesis of Te nanostructures and it is still a challenging issue to find convenient route to prepare Te nanostructures. Nonetheless, synthesis of Te nanostructures can be achieved by many approaches such as electrochemical deposition [19], microwave-assisted synthesis in ionic liquids [20], hydrothermal synthesis [21], and physical evaporation method [22]. Nevertheless, the preparation of Te nanostructures via wet chemistry routes is currently using. Mayers and Xia [23, 24] have successfully synthesized a series of uniform Te nanowires through the reduction of H₆TeO₆ or TeO₂ in different solvent systems by N₂H₄·H₂O and a refluxing process. Liu et al. [14, 25] reported the preparation of Te nanorods via reduction of (NH₄)₄TeS₄ in an aqueous solution by Na₂SO₃, in presence of sodium dodecyl benzenesulfonate (SDBS). Zhu et al. [26] have reported a developed microwave-assisted synthesis of Te nanorods and nanowires in ionic liquids by using TeO₂, PVP and BuPy⁺[BF₄]⁻. They found that both the ionic liquid and microwave heating play an important role in the formation of Te nanorods and nanowires. Shen et al. [27] synthesized Te rod-like crystals via a rapid polyol route by refluxing Na₂TeO₃ and (NH₃)₂S₂O₃ in ethylene glycol. In this

M. Panahi-Kalamuei · M. Salavati-Niasari (✉) · Z. Zarghami ·
M. Mousavi-Kamazani
Institute of Nano Science and Nano Technology, University
of Kashan, P.O. Box. 87317-51167, Kashan, Islamic Republic
of Iran
e-mail: salavati@kashanu.ac.ir

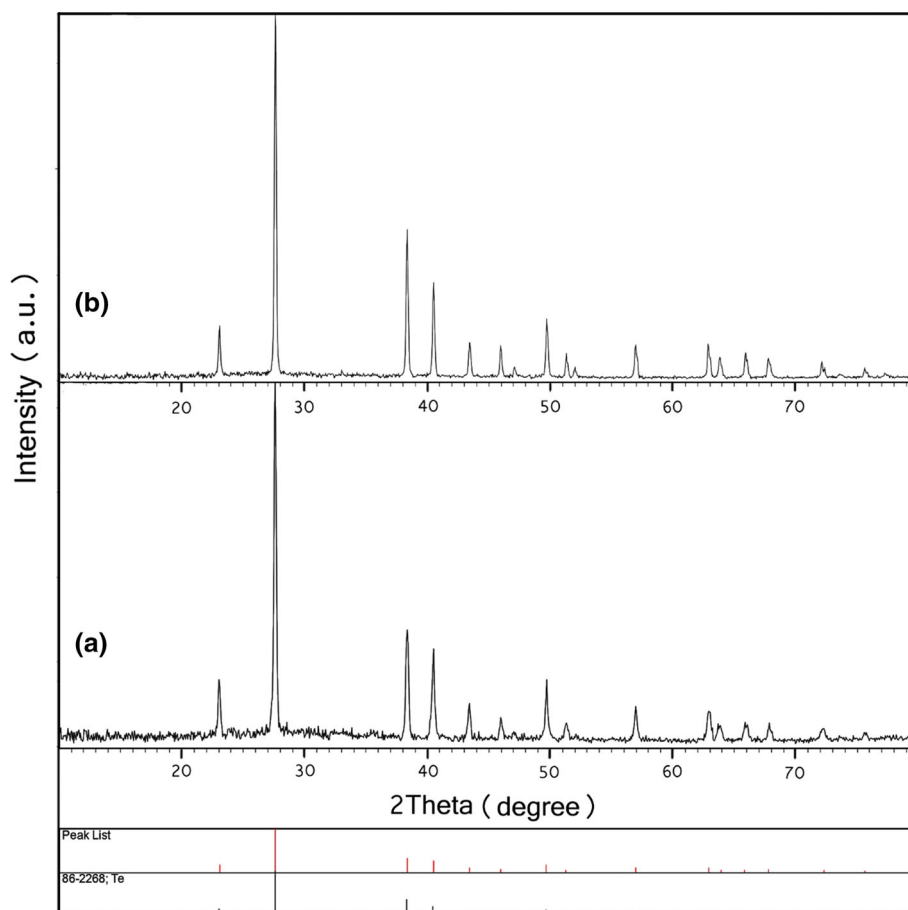
P. Rajabpour
Payame Noor Faculty of Science Tabriz, Tabriz, Iran

study, we synthesized Te nanostructures by employing microwave and sonochemical routes using TeCl_4 as a tellurium precursor and thioglycolic acid (TGA) as a reducing agent. TGA as a ‘soft template’ controls the morphology and plays a significant role in formation of nanostructures [28]. Additionally, effects of different parameters such as solvent and reducing agent on morphology and size were studied. A preliminary feasibility study on the developing a solar cell having the fluorine-doped tin oxide FTO/ TiO_2 /Te/Pt-FTO structure was also investigated.

Table 1 Experimental conditions used for preparation of Te nanostructures via microwave method

Sample no.	Reductan	Surfactant	Solvent
A1	Hydrazine	CTAB	Water
A2	Borohydride	CTAB	Water
A3	Hydrazine	TGA	Water
A4	Hydrazine	CTAB	Propylene glycol
A5	Hydrazine	TGA	TGA

Fig. 1 XRD pattern of the as-synthesized products at 750 W for 4 min in the presence of **a** $\text{N}_2\text{H}_4\cdot\text{H}_2\text{O}$ (sample A1), and **b** borohydride (sample A2)



2 Experimental

2.1 Materials and physical measurements

All of the chemicals used in the experiments were of analytical grade and used as received without further purification. TeCl_4 , KBH_4 , $\text{N}_2\text{H}_4\cdot\text{H}_2\text{O}$, TGA and cetyl trimethyl ammonium bromide (CTAB) were purchased from Merck Company. X-ray diffraction (XRD) patterns were recorded by a Philips-X’PertPro, X-ray diffractometer using Ni-filtered Cu $K\alpha$ radiation at scan range of $10 < 2\theta < 80$. Scanning electron microscopy (SEM) images were obtained on LEO-1455VP equipped with an energy dispersive X-ray spectroscopy. The energy dispersive spectrometry (EDS) analysis was studied by XL30, Philips microscope. The diffused reflectance UV–visible spectrum (DRS) of the sample was recorded by an Ava Spec-2048TEC spectrometer. Photocurrent density–voltage (J–V) curve was measured by using computerized digital multimeters (Ivium-n-Stat Multichannel potentiostat) and a variable load. A 300 W metal xenon lamp (Luzchem) served as assimilated sun light source, and its light intensity (or radiant power) was adjusted to simulated AM 1.5 radiation at 100 mW/cm^2 with a filter for this purpose.

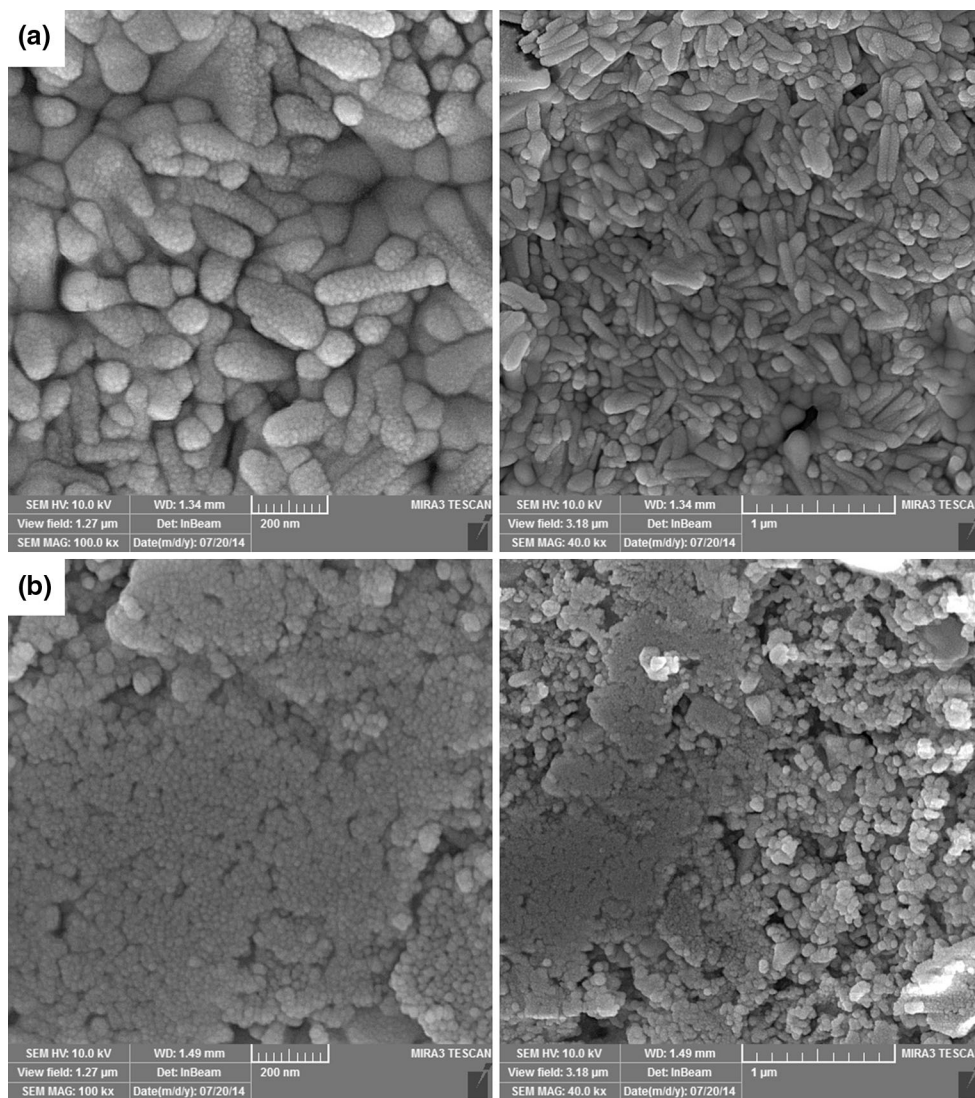


Fig. 2 SEM images of the products at 750 W for 4 min in the presence of different reducing agents **a** $\text{N}_2\text{H}_4\cdot\text{H}_2\text{O}$ (sample A1) and **b** KBH_4 (sample A2)

2.2 Preparation of Te nanostructures via microwave method

In a typical procedure, 0.2 mmol of TeCl_4 and 0.15 mmol of CTAB were dissolved in 38 ml distilled water stirring at room temperature for 5 min and then 2 ml hydrazine hydrate (1 M) was added to solution while stirred vigorously for 5 min. Finally obtained solution was microwave-heated at a power setting of 750 W for 4 min. The microwave oven followed a working cycle of 30 s on and 70 s off (30 % power). The obtained dark precipitate was washed with absolute ethanol and distilled water several times and was dried at 70 °C for 5 h. To study effects of reducing agent, solvent and etc. several experiments were designed. The experimental conditions are listed in Table 1.

2.3 Preparation of Te nanostructures via sonochemical method

In a typical procedure, 0.2 mmol of TeCl_4 was dissolved in 40 ml TGA. The obtained colorless solution was stirred at room temperature for 10 min and then was sonicated at a power setting of 60 W for 30 min. The obtained dark precipitate was washed with absolute ethanol and distilled water several times and was dried at 70 °C for 5 h (sample B).

2.4 Fabrication of FTO/ TiO_2 /Te/Pt-FTO cell

Electrophoresis deposition (EPD) was utilized to the prepare TiO_2 films [29–33]. During EPD, the cleaned FTO glass remained at a positive potential (anode) while a pure

steel mesh was used as the counter (cathode) electrode. The linear distance between the two electrodes was about 3 cm. Power was supplied by a Megatek Programmable DC Power Supply (MP-3005D). The applied voltage was 10 V. The deposition cycle was repeated four times, each time 5 s, and the temperature of the electrolyte solution was kept constant at 25 °C. The coated substrates were air dried. The apparent area of the film was $0.5 \times 0.5 \text{ cm}^2$. The obtained layer was annealed under an air flow at 500 °C for 30 min. Electrolyte solution and the amount of additives are important for creation a surface with high quality. Based on other experiment reported previously [29] we used optimal concentrations of additives in the electrolyte solution as follow: 120 mg/l of I_2 , 48 ml/l of acetone, and 20 ml/l of water. For deposition of Te powder on the FTO glass substrate, a paste of Te was initially prepared. The slurry was produced by mixing and grinding 1.0 g of the nano-sized Te with ethanol and water in several steps. Afterwards, the ground slurry was sonicated with ultra-sonic horn (Sonicator 3000; bande line, MS 72, Germany), and then mixed with terpeneol and ethyl cellulose as binders. After removing the ethanol and water with a rotary-evaporator, the final paste was prepared. The prepared Te paste was coated on TiO_2 film by a doctor blade technique [30–33]. After that the electrode was gradually heated under an air flow at 450 °C for 30 min. Counter-electrode was made from deposition of a Pt solution on FTO glass. Subsequently, this electrode was placed over TiO_2/Te electrode. Sealing was accomplished by pressing the two electrodes together on a double hot-plate at a temperature of about 110 °C. The redox electrolyte consisting of 0.05 M of LiI , 0.05 M of I_2 and 0.5 M of 4-tert-butylpyridine in acetonitrile as a solvent was introduced into the cell through one of the two small holes drilled in the counter electrode. Finally, these two holes were sealed by a small square of sealing sheet and characterized by I–V test.

3 Results and discussion

Figure 1a and b provide a comparison of typical XRD patterns of Te nanostructures derived from different reaction conditions for samples A1 and A2, respectively. The diffraction peaks, observed in Fig. 1, can be indexed to pure hexagonal phase of tellurium (space group: P3121) with cell constants $a = b = 4.4572 \text{ \AA}$, $c = 5.9290 \text{ \AA}$ and JCPDS No. 86-2268. The sharp diffraction peaks manifestation shows that the obtained Te nanostructures have high crystallinity. The crystallite sizes of the samples A1 and A2 estimated by the Scherrer formula shown in Eq. 1 [34–38] are 18 and 21 nm, respectively.

$$D(hkl) = k\lambda/\beta \cos \theta \quad (1)$$

where D is the crystallite size, as calculated for the (hkl) reflection, λ is the wavelength of $\text{Cu K}\alpha$ radiation (0.154178 nm), k is a constant related to the crystal shape (0.9), and β is the value of full width at half-maximum intensity (FWHM). The morphology of products was

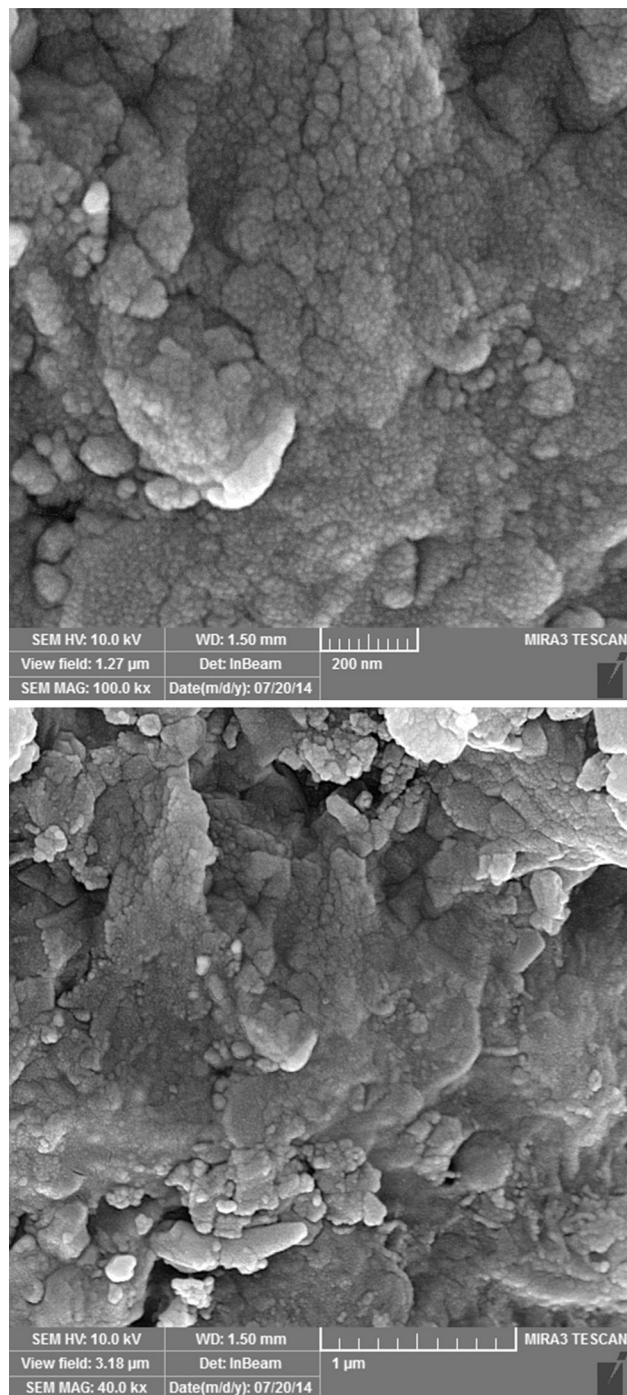


Fig. 3 SEM images of the products at 750 W for 4 min in the presence of hydrazine and thioglycolic acid (sample A3)

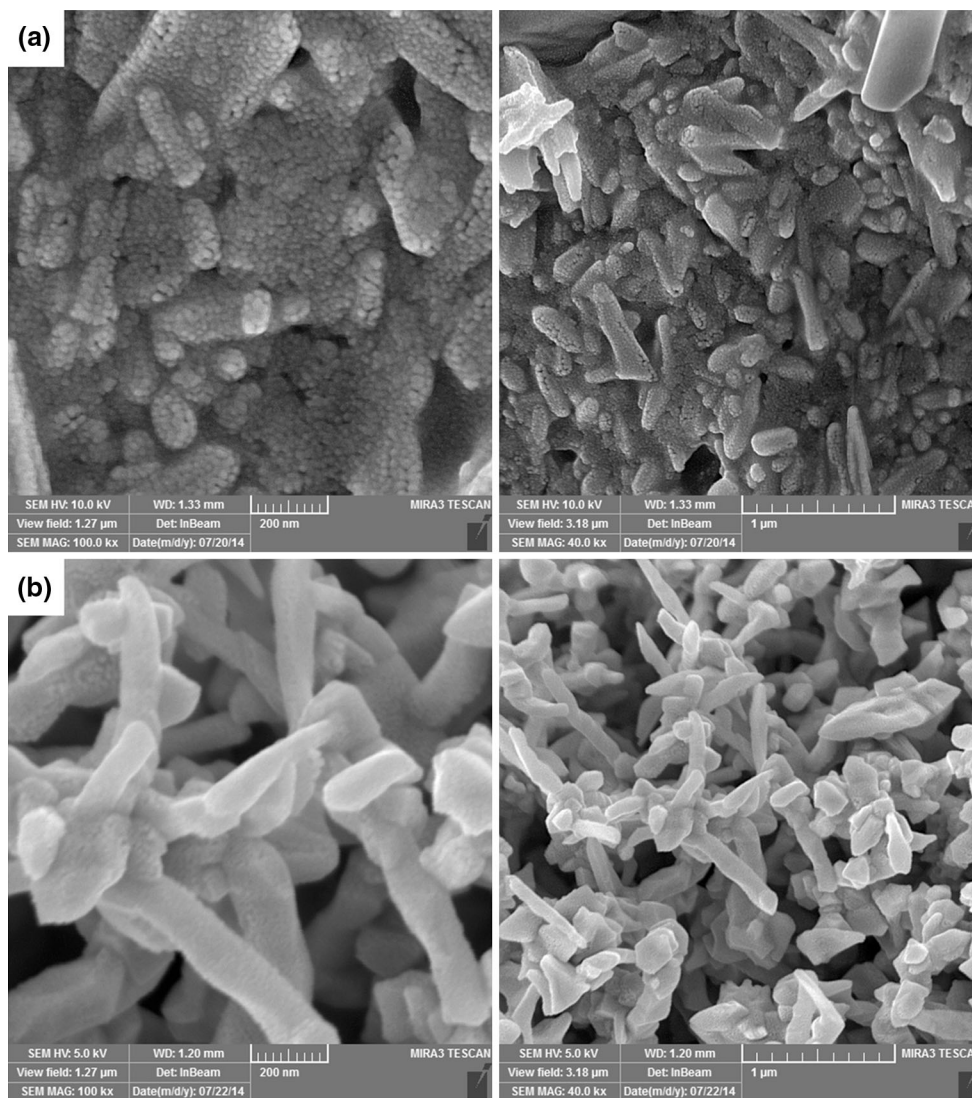
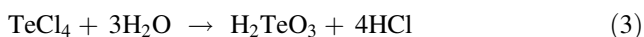
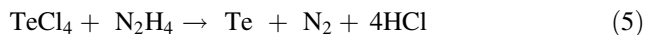


Fig. 4 SEM images of the products at 750 W for 4 min in the presence of different solvents instead of water **a** propylene glycol (sample A4), and **b** thioglycolic acid (sample A5)

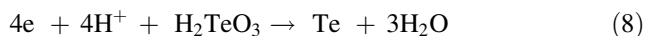
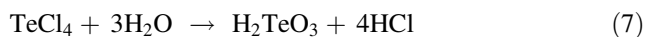
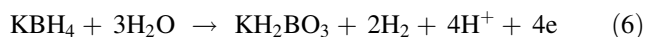
characterized by SEM. According to SEM images, the obtained products in our experiment are nanoparticles, sheets, rods and microparticles. In continue we will discuss in detail. In order to investigate the reducing agent effect on morphology and particle size, hydrazine and potassium borohydride were used (samples A1 and A2). As shown in Fig. 2a, nanorods mixed with nanoparticles were obtained by using of hydrazine (sample A1). Mechanism of tellurium nanostructures formation in the presence of hydrazine can be as follow:



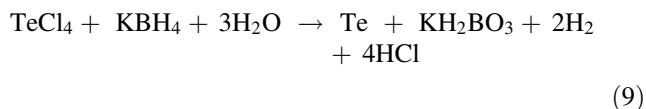
The final reaction:



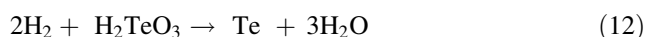
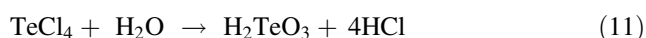
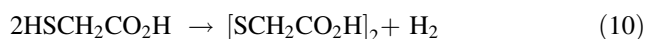
Using potassium borohydride (sample A2) leads to the aggregation and agglomeration of particles (Fig. 2b). Borohydride is stronger reducing agent than hydrazine and so in the presence of borohydride as a severe reducing agent that increases extremely nucleation rate, the spherical nanoparticles are formed as follow:



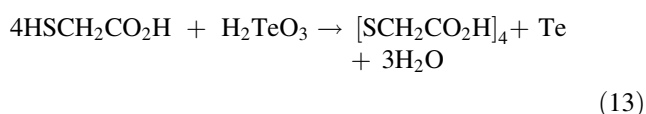
Final reaction:



For studying of surfactant effects on the Te nanostructures prepared via microwave method, the reaction was performed in the presence of 0.2 ml TGA (sample A3). Under this condition, the morphology changed and the rod-like self-assembly orders of nanoparticles was disappeared as well as spherical nanoparticles with smaller size was formed that was agglomerated at some points (Fig. 3). The agglomeration can be caused to effect of TGA on the mechanism of reaction because TGA can play reducing agent role too. Therefore, TGA can increase the nucleation rate. The mechanism of tellurium nanostructures formation in the presence of TGA can be as follow:



Final reaction:



To investigate the solvent effect, propylene glycol (sample A4) and TGA (sample A5) were used instead of water (Fig. 4a, b, respectively). The nanostructures prepared in the propylene glycol are nearly similar to nanostructured prepared in water (Fig. 4a) with difference that the nanostructures prepared in the propylene glycol have less order for forming of nanorods. This could be because of the greater dielectric loss factor of propylene glycol resulting in the faster reaction rate than water. Nano rod-like shapes were obtained when the reaction was carried out in the presence of TGA as solvent, surfactant and reducing agent (Fig. 4b). TGA has $-\text{SH}$ and $-\text{COOH}$ functional groups. When the excess amount of TGA is used, TGA is adsorbed on the surface of Te nanoparticles through hydrogen and S–S bonds. Therefore, Te nanoparticles are linked together chain likely through hydrogen and S–S bonds of TGA and finally form the rod-like Te nanostructures.

One of main issues affecting the morphology and size is type of preparation route. Therefore the preparation of Te nanostructure via sonochemical method was studied. For this reason, the A5 experiment was repeated via sonochemical method at a power setting 60 W for 30 min (sample B). In this condition the nanoparticles were obtained (Fig. 5) while rod-like nanostructures were obtained

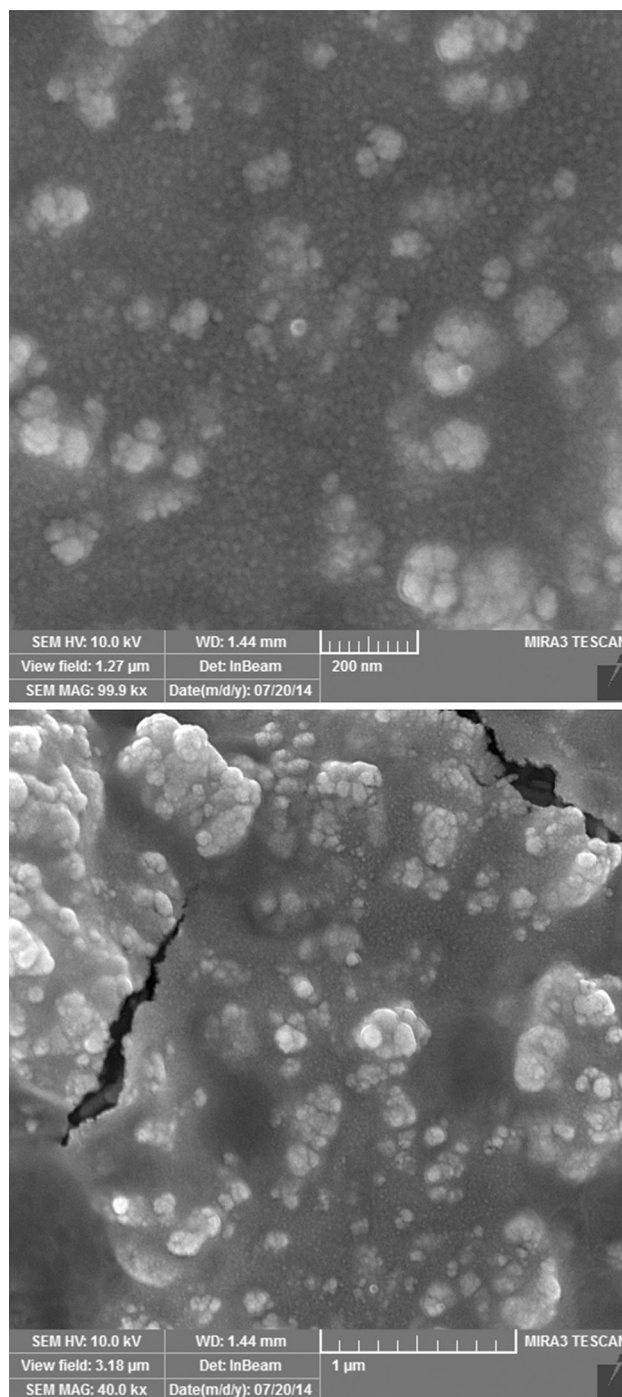


Fig. 5 SEM images of the as-synthesized product via sonochemical route (sample B)

via microwave method (Fig. 4b). Any type of preparation method has its nucleation and growth mechanism and as a result, provides products with various size and morphologies. XRD pattern of the sample obtained by sonochemical approach (sample B, Fig. 6) confirmed that this sample is in the same crystalline phase with those obtained by

Fig. 6 XRD pattern of the as-synthesized product via sonochemical route (sample B)

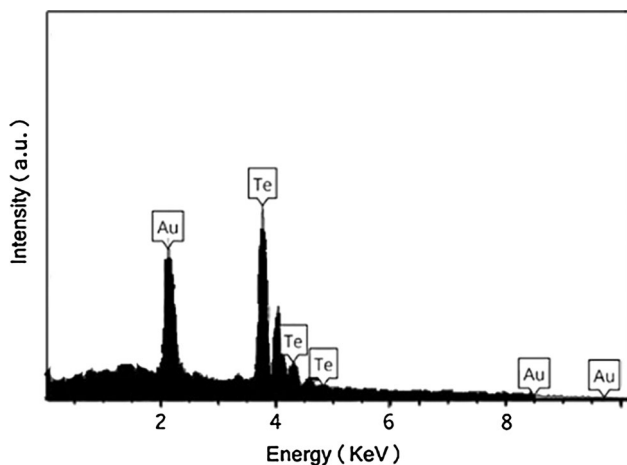
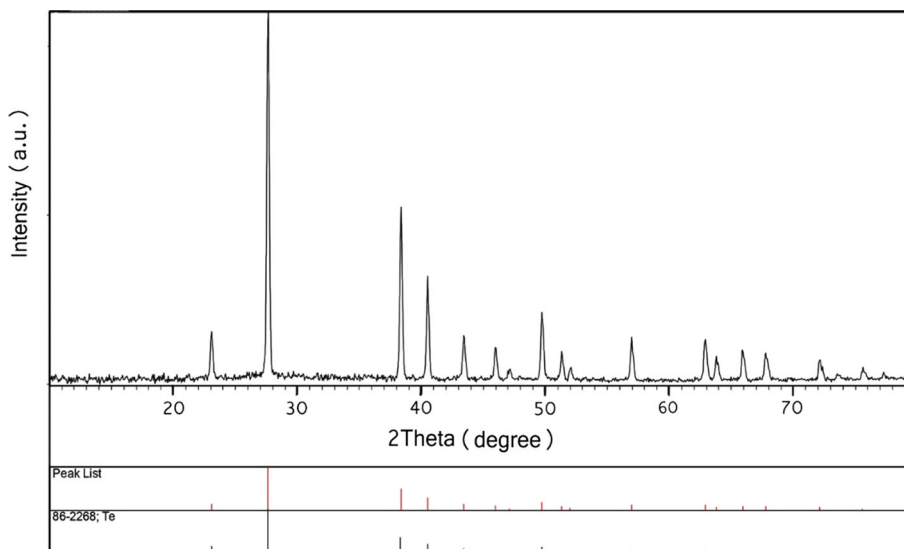


Fig. 7 EDX spectrum of the as-synthesized product via sonochemical route (sample B)

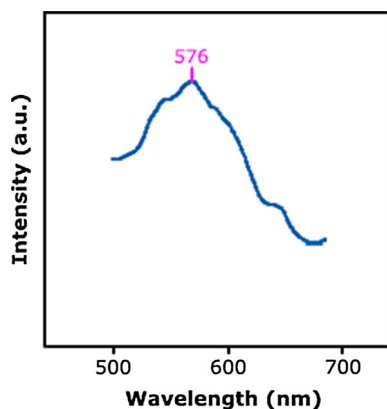
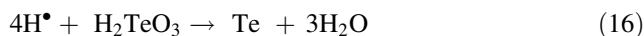
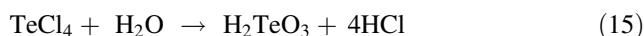
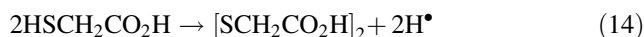
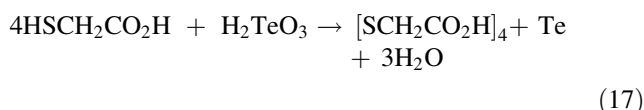


Fig. 8 Diffuse reflectance spectrum of Te nanoparticles (sample A1)

microwave method whereas the average crystal diameter is different. EDX analysis was used to identify the elemental composition of Te nanostructures (sample B, Fig. 7), indicating that only Te peaks exist in the samples except the peak relating to the use of a Au-coated substrate for samples examination. Therefore, both XRD and EDX analyses revealed that pure Te were successfully synthesized by the current synthetic route. Reaction performed for preparation of Te nanostructures via sonochemical method in the presence of TGA:



Final reaction:



The UV–Vis absorption spectrum of the as-synthesized Te nanocrystals (sample A) was recorded as shown in Fig. 8. The absorption edge of obtained Te nanostructures is observed at 576 nm (2.15 eV) that is in good agreement with the literature [39]. According to the Hartree–Fock–Slater study, there are two possible peaks in the range from 250 to 800 nm. Among them, the peak in the range of 3–6 eV is due to the allowed direct transition from the valence band (p-bonding VB2) to the conduction band (p-antibonding CB1), and another peak in the range of 0–3 eV can be assigned to a forbidden direction transition from the valence band (p-lone-pair VB3) to the conduction band (p-antibonding CB1) [39]. Therefore, the peak located

Fig. 9 J - V characterization of prepared solar cells **a** sample A1, **b** sample A2, **c** sample A5, and **d** sample B

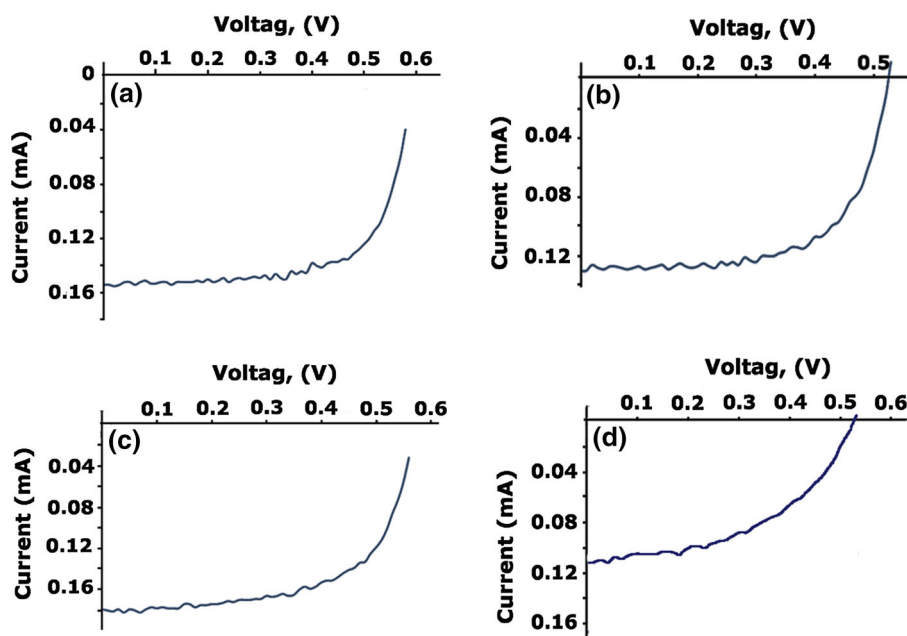


Table 2 J - V characteristic of prepared solar cells by Te

Sample no.	I_{sc} (mA)	J_{sc} (mA/cm ²)	V_{oc}	FF	η (%)
A1	0.156	0.312	0.59	0.7	0.13
A2	0.132	0.264	0.53	0.64	0.09
A5	0.181	0.392	0.56	0.59	0.13
B	0.111	0.222	0.53	0.49	0.06

at 576 nm (2.15 eV) is assigned to the allowed direct transition. However, the peak of the forbidden transition does not exist in Fig. 8. This may be due to the diameter of the Te nanorods, because the position and intensity of the two peaks are affected by the diameter and length of 1D tellurium nanostructures [39]. The peak of the forbidden transition exists in the absorption spectrum when the diameter of 1D tellurium nanostructure is below 25 nm [39]. In our work, the average diameter of Te nanorods is about 70 nm. Therefore, the peak of the forbidden transition is absent in Fig. 8. Current-voltage characteristic of FTO/TiO₂/Te/Pt-FTO cells (Fig. 9) for some samples was studied. The results are listed in the Table 2. As can be seen, different efficiencies are obtained for samples with different shapes and sizes. For an example, the highest efficiency is achieved by nanorods prepared via microwave method (sample A1) while the lowest efficiency is achieved by agglomerated products obtained via sonochemical route (sample B). Stronger electric fields within bonds result in higher open circuit voltage. To obtain a strong electric field, difference between Fermi levels of two materials (p and n) must be large. For this purpose, semiconductors energy gap must be large. Therefore, open

circuit voltage of a solar cell will increase with its energy gap. Although, increasing the energy gap leads to fewer photon could generate electron-hole pairs and as a result, less short-circuit current will be generated. Therefore, increasing energy gap and actually increasing particle size have different effects on open-circuit voltage and short-circuit current. In this respect, an optimal particle size for obtaining high efficiency is offered. Morphology has also effect on efficiency by exposing different surface areas to the light.

In comparison to other similar works, our method is simpler, faster, and more controllable. We have used TeCl₄ as a new Tellurium source to prepare the Te nanostructures. Furthermore, TeCl₄ is a good Tellurium source, which dissolves well in distilled water and provides a highly reactive in aqueous solution. In our experiment, when TeCl₄ is added in deionized water, a completely clear acidic solution is obtained that contains H₂TeO₃; however, H₂TeO₃ can be quickly converted to Te by hydrazine, potassium borohydride, and TGA. As a result, TGA can reduce TeCl₄ to Te, where no other reducing agent is needed. Finally, solar cell efficiency of products were studied by different chemical methods and it was found that morphology and size have significant effect on efficiency.

4 Conclusions

In the summary, Te nanostructures with various shapes have been prepared via two facile and rapid synthesis methods, microwave and sonochemical routes, with TGA

as a new reducing agent for reducing TeCl_4 to Te. In this work, the effect of reducing agent, solvent and surfactant on the morphology and particle size of the products was investigated. To fabricate a FTO/ TiO_2 /Te/Pt-FTO solar cell, Te film was directly deposited on top of the TiO_2 . Solar cell results indicate that there is the possibility of developing an inexpensive solar cell by tellurium produced by these methods. The prepared Te products were characterized extensively by means of XRD, EDX, SEM and DRS.

Acknowledgments Authors are grateful to the council of University of Kashan for supporting this work by Grant No. 159271/265.

References

1. S. Fukuda, T. Shiosaki, A. Kawabata, in *Ultrasonics Symposium* 9 (1979)
2. K. Ariki, T. Tanaki, *Jpn. J. Appl. Phys.* **11**, 472 (1972)
3. Y. Wang, Z. Tang, P. Podsiadlo, Y. Elkasabi, J. Lahann, N. Kotov, *Adv. Mater.* **18**, 518 (2006)
4. S. Fujiwara, T.S. Ike, K. Okada, M. Aoki, N. Kambe, N. Sonoda, *Tetrahedron Lett.* **33**, 7021 (1992)
5. D. Tsiulyanu, S. Marian, V. Miron, H.D. Liess, *Sens. Actuators B Chem.* **85**, 232 (2002)
6. S. Sen, K.P. Muthe, N. Joshi, S.C. Gadkari, S.K. Gupta, M. Roy, S.K. Deshpande, J.V. Yakhmi, *Sens. Actuators B Chem.* **98**, 154 (2004)
7. P. Bodiul, N. Bondarchuk, T. Huber, L. Konopko, A. Nikolaeva, O. Botnari, in *25th International Conference on Thermoelectrics*, 607 (2006)
8. G. Henshaw, I.P. Parkin, G.A. Shaw, *J. Chem. Soc. Dalton Trans.* **2**, 231 (1997)
9. Y.D. Li, H.W. Liao, Y. Ding, Y. Fan, Y. Zhang, Y.T. Qian, *Inorg. Chem.* **38**, 1382 (1999)
10. R. Zheng, W. Cheng, E. Wang, S. Dong, *Chem. Phys. Lett.* **395**, 302 (2004)
11. X.Y. Gao, T. Gao, L.D. Zhang, *J. Mater. Chem.* **13**, 6 (2003)
12. B. Gates, Y.D. Yin, Y.N. Xia, *J. Am. Chem. Soc.* **122**, 12582 (2000)
13. Y.T. Chen, Q.Y. Sun, H.L. Li, *Chem. Lett.* **32**, 448 (2003)
14. Z.P. Liu, Z.K. Hu, J.B. Liang, S. Li, Y. Yang, S. Peng, Y.T. Qian, *Langmuir* **20**, 214 (2004)
15. X.Y. Liu, M.S. Mo, J.H. Zeng, Y.T. Qian, *Cryst. J. Growth* **259**, 144 (2003)
16. J. Lu, Y. Xie, F. Xu, L.Y. Zhu, *J. Mater. Chem.* **12**, 2755 (2002)
17. H. Zhang, D.R. Yang, Y.J. Yi, X.Y. Ma, J. Xu, D.L. Que, *J. Phys. Chem. B* **108**, 1179 (2004)
18. Y.J. Zhu, X.L. Hu, *Mater. Lett.* **58**, 1234 (2004)
19. A.W. Zhao, C.H. Ye, G.W. Meng, L.D. Zhang, P.M. Ajayan, *J. Mater. Res.* **18**, 2318 (2003)
20. Y.J. Zhu, W.W. Wang, R.J. Qi, X.L. Xu, *Angew. Chem. Int. Ed.* **43**, 1410 (2004)
21. M.S. Mo, J.H. Zeng, X.M. Liu, W.C. Yu, S.Y. Zhang, Y.T. Qian, *Adv. Mater.* **14**, 1658 (2002)
22. X.L. Li, G.H. Cao, C.M. Feng, Y.D. Li, *J. Mater. Chem.* **14**, 244 (2004)
23. B. Mayers, Y.N. Xia, *J. Mater. Chem.* **12**, 1875 (2002)
24. B. Mayers, Y.N. Xia, *Adv. Mater.* **14**, 279 (2002)
25. Z.P. Liu, Z.K. Hu, Q. Xie, B.J. Yang, J. Wu, Y.T. Qian, *J. Mater. Chem.* **13**, 159 (2003)
26. Y.J. Zhu, W.W. Wang, R.J. Qi, X.L. Hu, *Angew. Chem.* **116**, 1434 (2004)
27. G. Shen, D. Chen, K. Tang, Y. Qian, *Mater. Res. Bull.* **39**, 2077 (2004)
28. M. Panahi-Kalamuei, M. Mousavi-Kamazani, M. Salavati-Niasari, *Mater. Lett.* **136**, 218 (2014)
29. M. Hamadani, V. Jabbari, A. Gravand, M. Asad, *Surf. Coat. Technol.* **206**, 4531 (2012)
30. M. Panahi-Kalamuei, M. Mousavi-Kamazani, M. Salavati-Niasari, S.M. Hosseinpour-Mashkani, *Ultrason. Sonochem.* **23**, 246 (2015)
31. M. Mousavi-Kamazani, M. Salavati-Niasari, M. Sadeghinia, *Mater. Lett.* **142**, 145 (2015)
32. M. Panahi-Kalamuei, F. Mohandes, M. Mousavi-Kamazani, M. Salavati-Niasari, Z. Fereshteh, M. Fathi, *Mater. Sci. Semicond. Process.* **27**, 1028 (2014)
33. M. Panahi-Kalamuei, M. Salavati-Niasari, S.M. Hosseinpour-Mashkani, *J. Alloys Compd.* **617**, 627 (2014)
34. M. Mousavi-Kamazani, M. Salavati-Niasari, *Compos. Part B-Eng.* **56**, 490 (2014)
35. M. Mousavi-Kamazani, M. Salavati-Niasari, M. Sadeghinia, *Superlattices Microstruct.* **63**, 248 (2013)
36. M. Mousavi-Kamazani, M. Salavati-Niasari, M. Ramezani, *J. Clust. Sci.* **24**, 927 (2013)
37. M. Salavati-Niasari, S. Alizadeh, M. Mousavi-Kamazani, N. Mir, O. Rezaei, E. Ahmadi, *J. Clust. Sci.* **24**, 1181 (2013)
38. M. Mousavi-Kamazani, M. Salavati-Niasari, H. Emadi, *Mater. Res. Bull.* **47**, 3983 (2012)
39. H.H. Li, P. Zhang, C.L. Liang, J. Yang, M. Zhou, X.H. Lu, G.A. Hope, *Cryst. Res. Technol.* **47**, 1069 (2012)